Static compression of B2 KCl to 230 GPa and its P-V-T equation of state

Revision 1

Static compression of B2 KCl to 230 GPa and its *P-V-T* equation of state

SHIGEHIKO TATENO[1,*], TETSUYA KOMABAYASHI[2], KEI HIROSE[1,3], NAOHISA HIRAO[4], AND YASUO OHISHI[4]

[1]Earth-Life Science Institute, Tokyo Institute of Technology, 2-12-1 Ookayama, Meguro, Tokyo 152-8550, Japan
[2]School of GeoSciences and Centre for Science at Extreme Conditions, University of Edinburgh, Grant Institute, The King's Buildings, James Hutton Road, Edinburgh EH9 3FE, U.K.
[3]Department of Earth and Planetary Science, The University of Tokyo, 7-3-1 Hongo, Bunkyo, Tokyo 113-0033, Japan
[4]Japan Synchrotron Radiation Research Institute, 1-1-1 Kouto, Sayo-cho, Hyogo 679-5198, Japan

ABSTRACT

The pressure-volume-temperature (*P-V-T)* measurements of the B2 (CsCl-type) phase of KCl were performed at 9–61 GPa / 1500–2600 K and up to 229 GPa at room temperature, based on synchrotron X-ray diffraction measurements in a laser-heated diamond-anvil cell (DAC). The nonhydrostatic stress conditions inside the sample chamber were critically evaluated based on the platinum pressure marker. With thermal annealing by laser after each pressure increment, the deviatoric stress was reduced to less than 1% of the sample pressure even at the multi-Mbar pressure range. The obtained *P-V-T* data were fitted to the Vinet equation of state with the Mie-Grüneisen-Debye model for thermal pressure. The Grüneisen parameter at ambient condition was found to be as small as 0.58(±0.05), which represents a small thermal pressure. Such a low thermal pressure validates the use of a KCl pressure medium as a pressure marker at high temperatures.

Key words: KCl, equation of state, high pressure, DAC

---

* E-mail: tateno@elsi.jp (S. Tateno)

INTRODUCTION

Potassium chloride is often used as a pressure gauge and pressure-transmitting medium in high-pressure experiments using a DAC because it hardly reacts with silicates and metals and provides lesser deviatoric stress inside the sample chamber. Moreover, it can be used for very high temperature experiments such as melting experiments (e.g., Anzellini et al. 2013; Andrault et al. 2014; Morard et al. 2017), since the melting temperature of KCl is much higher than that of NaCl (Boehler et al. 1997). KCl is also useful for synchrotron-based experiments when the X-ray beam is accurately aligned to a heating laser beam spot as X-ray induces visible fluorescent light in KCl in a wide pressure range, although the diffraction peaks are stronger compared to NaCl.

The B1-phase of KCl with the NaCl-type structure transforms into the B2 (CsCl-type) structure at 2 GPa (Walker et al. 2002). Equations of state (EoS) of B2 KCl have been proposed from experimental studies in a multi-anvil press or DAC (Yagi 1978; Campbell and Heinz 1991; Walker et al. 2002; Dewaele et al. 2012). Cold compression experiments on KCl in a helium pressure medium performed up to 160 GPa reported its highly compressible nature comparable to solid argon (Dewaele et al. 2012). Walker et al. (2002) reported that B2 KCl exhibits low thermal expansivity up to 8 GPa and 873 K, which was supported by recent theoretical calculations by Dewaele et al. (2012). The low thermal expansivity may provide the opportunity for KCl to serve as a practical pressure standard at high temperature even when it is used as a pressure medium; namely, a large temperature gradient, if any, across the pressure medium may not matter when calculating the sample pressure from its *P*-*V*-*T* EoS. Hence, precise evaluation of its thermal EoS is

of great importance for high *P-T* experiments in the DAC. Here we present a new EoS for B2-type KCl from our high *P-T* experiments to 230 GPa/300K and 60 GPa/2600 K in a laser-heated DAC.

EXPERIMENTAL METHODS

High *P-T* conditions were generated using laser-heated DAC techniques. Diamond–anvils with a culet size of 300, 120, or 40 μm were used depending on the target pressure. The starting material was powder of KCl (Wako Pure Chemical Industries, Ltd., 99.5% purity) which was mixed with platinum black that served as an internal pressure standard and laser absorber. The sample mixture was loaded into a hole drilled in a Re-gasket together with insulation layers. We used SiO_2 glass (runs #1 and #2) or argon (runs #5 and #6) for thermal insulation. Argon was cryogenically loaded into the sample chamber. The sample assembly was then dried by leaving the cell in a vacuum oven at 393 K for >1 h prior to pressurizing, and flushed with argon gas when the oven was opened. The sample pressure was calculated from the unit-cell volume of Pt based on the EoS proposed by Sokolova et al. (2016).

Angle-dispersive XRD measurements were conducted at BL10XU, SPring-8 (Ohishi et al. 2008). XRD patterns were collected on an imaging plate (*Rigaku R-AXIS IV*). The typical exposure time was 2 min. Monochromatic incident X-rays were focused by stacked compound refractive lenses and collimated to an area of approximately 6–μm full-width at half maximum (FWHM) at the sample position. The wavelength was precisely determined during each beamtime using a CeO_2 standard: 0.4133–0.4135 Å (~30 keV). Two-dimensional XRD images were integrated over the Debye–Scherrer

rings using the IPAnalyzer program (Seto et al. 2010) in order to produce conventional one-dimensional diffraction patterns as a function of two-theta angle. The obtained peak profiles and backgrounds were fit to pseudo-Voigt line shapes within the software package of PDindexer (Seto et al. 2010). The lattice parameters were obtained by a least-squares fit of peak positions. The unit-cell volumes were determined by averaging lattice parameters from 3–6 peaks and 2–5 peaks for Pt and B2 KCl, respectively after careful selection based on stress analysis (see below). Weak or poorly resolved diffraction peaks were not used in volume determination or stress analysis. Heating was performed from both sides of the sample by employing a pair of 100 W single-mode Yb fiber lasers (*SPI*). Temperatures were measured by a spectroradiometric method (Ohishi et al. 2008). In order to reduce the radial temperature gradient, we used beam shapers (*New focus*) that convert a beam with a Gaussian intensity distribution to one with a flat-top distribution. The sample temperatures reported in this study are the average in the 6–μm region probed by X-rays around the hot spot.

RESULTS AND DISCUSSION

Four separate sets of experiments were performed to measure the unit-cell volume of B2 KCl and Pt at 84.8–229 GPa at 300 K (runs #1 and 2) and 4.2-59.4 GPa at 300-2560 K (runs #3 and 4). The observed unit-cell parameters and volumes are summarized in Table 1. Representative XRD patterns are shown in Fig. 1, in which diffraction peaks from B2 KCl, Pt, and Ar pressure medium were found. Diffraction peaks from SiO_2 were not observed through the present experiments; crystallization of SiO_2 glass is known to be quite sluggish (Komabayashi et al. 2012; Tateno et al. 2015). We employed laser heating

in order to reduce potential deviatoric stress in the sample as well as to measure the sample volume at high temperatures. The laser beam was carefully rastered over the whole sample at 1300–4000 K for 5–10 min depending on the pressure. We measured the unit-cell volume at 300 K after thermal annealing. The diffraction peaks from B2 KCl and Pt became sharp due to heating and spotty reflections also appeared on the diffraction rings. The following compression at room temperature significantly broadened the peaks and some of the diffraction spots disappeared, particularly for B2 KCl (Supplemental Fig. S1). This is likely due to reduction in the grain size and/or increase of micro-stresses as discussed below. Subsequently, the sharp and spotty diffractions were again observed on laser heating. The grain growth of B2 KCl was confirmed up to 250 GPa and 3500 K, suggesting its thermodynamic stability.

Nonhydrostaticity

Potential sources for the systematic errors in the unit-cell volume measurement include the presence of nonhydrostatic stress conditions induced by uniaxial compression in the DAC. Here we evaluated the nonhydrostatic stress conditions inside the sample chamber from diffraction line shifts and peak widths before/after heating. Uniaxial compression develops the differential stress, *t*, defined as the difference between the maximum stress along the compression axis and the minimum stress in the radial direction. The differential stress results in variation in the lattice parameter as a function of crystallographic orientation (*hkl*). Sing and Takemura (2001) proposed a linear relation between the measured lattice parameter for a given *hkl*, $a_m(hkl)$, and $3(1\text{-}3\sin^2\theta)\Gamma(hkl)$, referred to as the gamma plot, where θ is the diffraction angle and $\Gamma(hkl) = (h^2k^2 + k^2l^2 + l^2h^2)/(h^2 + k^2 + l^2)^2$. The *St* value can be derived directly from the intercept (M_0) and slope

(M_1) of the gamma plot: $St = -3M_1/M_0$, where S is the single-crystal elastic compliance. The differential stress in platinum can be calculated with the pressure dependence of the S value from the theoretical study (Menéndez-Proupin and Singh 2007). On the other hand, since S of B2 KCl is not available under pressure, we examined the St value for B2 KCl as a stress indicator. The gamma plots for Pt and KCl at selected pressures are shown in Figure 2. The slope was significantly reduced by laser annealing for both materials. The differential stress measured in Pt at 229 GPa, the highest pressure achieved in this study, was as small as 0.7 GPa after annealing. The t values observed after heating in this study were up to 1% of the pressure. These are much lower than the t values measured in the cold compression using a He pressure medium (Dorfman et al. 2012). Similarly, the laser heating decreased the magnitude of the St value of KCl. $|St|$ obtained to 100 GPa typically ranged from 0 to 0.005, and increased to 0.012 at 229 GPa. In particular, the lattice parameters calculated from each of the (200) and (400) lines of Pt are largely deviated, implying that these reflections are most affected by uniaxial compression. This observation is commonly observed in previous experimental studies on cubic phases such as platinum, gold, and $CaSiO_3$ perovskite (Shim et al. 2000; Takemura and Dewaele 2008; Sakai et al. 2011; Dorfman et al. 2012). Similarly, the gamma plots for B2 KCl indicate that the effect of the uniaxial stress is largest for $a_m(200)$. Figure 3 shows the variation of the t and St values of Pt and KCl, respectively, which were measured before/after laser hearing. The deviatoric stress always developed upon compression at room temperature, leading to scattered data points. Subsequent laser heating clearly made the stress smaller, although greater compressions >100 GPa showed larger deviatoric stresses even after laser annealing. In summary, (i)the thermal annealing made in our

experiments reduced the deviatoric stress and (ii)the use of the (200) and (400) lines of Pt and the (200) line of B2 KCl introduces systematic errors in the calculated unit-cell volumes. The selection of the diffraction lines based on the gamma plot can minimize the nonhydrostatic effect on volume determination (Takemura and Dewaele 2008; Dewaele et al. 2012). Due to (ii), we did not use the (200) and (400) lines of Pt and the (200) line of B2 KCl.

The width of a powder diffraction line (*hkl*) is related to the micro-stresses in a powder material (inter-grain stress) and grain size (e.g., Sing et al. 2008). Figure 4 shows the FWHM of the most intense reflections of (111) line and (110) line from Pt and KCl, respectively, normalized to the diffraction angle 2θ as a function of pressure. The FMHM of both Pt and KCl significantly decreased upon laser heating, suggesting grain growth or reduced micro-stress which is at a similar level to that observed in the CeO_2 standard comparable to instrumental resolution. We note that laser heating is very useful to reduce macro/micro stresses in the sample (e.g., Uts et al. 2013). The FWHM observed at 6–18 GPa was anomalously large even after heating, although the measured deviatoric stresses indicates quasi-hydrostatic conditions (Fig. 3a). This observation suggests the micro-stress resulting from grain contact is relatively large under such small compression, even if the aggregate itself is hydrostatically compressed. The systematic increase of FWHM on compression is likely caused by a combined effect of the decreased grain size and increased micro-stress.

As mentioned above, we made efforts to minimize the effects of the deviatoric stress by employing thermal annealing and choosing the diffraction lines for calculating the unit-cell volume. As a result, our *P*–*V*–*T* data in Table 1 represent much lesser

nonhydrostatic conditions than in the case of a He pressure medium without thermal annealing (Figs. 3 and 4).

Equation of state at room temperature

We collected unit-cell volume data at 300 K up to 229 GPa, all after thermal annealing. The measured *P*–*V* data were fitted to the Vinet EoS (Fig. 5a):

$$P(V,T_0) = 3K_0\left(\frac{V}{V_0}\right)^{-2/3}\left[1-\left(\frac{V}{V_0}\right)^{1/3}\right] exp\left\{\frac{3}{2}(K'_0-1)\left[1-\left(\frac{V}{V_0}\right)^{1/3}\right]\right\} \quad (1)$$

where V_0, K_0, and K'_0 are the unit-cell volume, isothermal bulk modulus, and its pressure derivative at the reference *P*–*T* condition that is 1 bar and 300 K. In the fitting procedure, due to the lack of sufficient data at low pressure near ambient condition in this study, we fixed V_0 at 54.5 Å^3 from the literature (Dewaele et al. 2012) which was precisely constrained under hydrostatic condition below 10 GPa with a single crystal KCl loaded in liquid He. We then fitted all the remaining parameters simultaneously, including thermoelastic parameters mentioned below. The fitting yielded K_0 and K'_0 to be 18.3 ± 0.3 GPa and 5.60 ± 0.03, respectively, based on the Pt pressure scale by Sokolova et al. (2016). Another fitting based on Holmes et al. (1989)'s Pt scale leads to similar values of K_0 = 17.4 ± 0.2 GPa and K'_0 = 5.76 ± 0.03. The fitting results are summarized in Table 2. Our compression curve is in good agreement with the recent results by Dewaele et al. (2012) to ~50 GPa, above which the two curves however deviate from each other slightly (Fig. 5a). Figure 6a compares the calculated pressure between the previous EoS reported by Dewaele et al. (2012) and ours with calibration against various Pt scales (Holmes et al. 1989; Dorogokupets and Oganov 2007; Yokoo et al. 2009; Ono et al. 2010; Dorfman et al.

2012). A precise comparison on the EoS of KCl between Dewaele et al. (2012) and ours may be made using the curve from Dorogokupets and Oganov (2007)'s Pt scale in Fig. 6a, as Dewaele et al. (2012) used the ruby scale proposed by Dorogokupets and Oganov (2007). The comparison indicates that our EoS gives a lower pressure at a given volume of KCl. In other words, our compression curve gives a smaller volume at a given pressure, which may arise due to the different stress state developed in the sample chamber. Dewaele et al. (2012) used a single crystal of KCl loaded in He. Helium is known to be a good pressure-transmitting medium even after solidification above 10 GPa. As we discussed above, our *P*–*V*–*T* data represent lesser nonhydrostatic conditions than experiments with a He pressure medium without thermal annealing (Dorfman et al. 2012). Also, Takamura and Dewaele (2008) reported the stress state of gold loaded in He medium, and argued that the deviation from the hydrostatic condition becomes prominent under high pressure, particularly at Mbar pressures.

Thermal equation of state

To construct a thermal EoS for B2 KCl, all the high-temperature data were analyzed in the framework of a thermal pressure EoS. At a constant sample volume, the following equation holds

$$P(V,T) = P(V,T_0) + \Delta P_{th} \quad (2)$$

where ΔP_{th} is the thermal pressure term. We evaluated the thermal pressure term based on the Mie–Grüneisen–Debye model (e.g., Jackson and Rigden 1996)

$$\Delta P_{th} = \frac{\gamma}{V}[E_{th}(V,T) - E_{th}(V,T_0)] \quad (3)$$

where γ and E_{th} are the Grüneisen parameter and internal thermal energy, respectively. The thermal energy is calculated from the Debye approximation

$$E_{th} = \frac{9nRT}{(\theta/T)^3}\int_0^{\theta/T}\frac{x^3}{e^x-1}dx \quad (4)$$

where n and R, and θ are the number of atoms per formula unit, gas constant, and Debye temperature, respectively. The volume dependence of Grüneisen parameter (q) is expressed as

$$\gamma(V) = \gamma_0\left(\frac{V}{V_0}\right)^q \quad (5)$$

$$\theta = \theta_0 exp\{[\gamma_0 - \gamma(V)]/q\} \quad (6)$$

where θ_0 and γ_0 are the Debye temperature and Grüneisen parameter at ambient condition, respectively. Fitting all the high temperature data simultaneously yielded γ_0 = 0.58 ± 0.05 and q = 0.9 ± 0.2 with θ_0 fixed at 235 K (Gray 1963). Calculated isothermal compression curves from this model and the *P*–*V*–*T* data are presented in Figure 4b. We also evaluated the EoS based on Holmes et al. (1989)'s Pt scale (Table 2). The obtained Grüneisen parameter is again as small as 0.46 ± 0.05 with q = 0.7 ± 0.3. The fitted parameters are listed in Table 2.

Another thermal pressure EoS, which is known as the thermodynamic thermal pressure model (Jackson and Rigden 1996), was also employed. In this EoS, instead of Eq. (3), the following equation is applied

$$\Delta P_{th} = \int_{T_0}^{T}[\alpha K_T]_V dT \cong \alpha K_T(T - T_0) \quad (7)$$

where α is the volumetric thermal expansivity, and K_T is the isothermal bulk modulus. Here αK_T was assumed to be a constant, which is reasonable when the temperature range is much higher than the Debye temperature (235 K for KCl). The fitting of all the data yielded αK_T = 0.0037 ± 0.0001 GPa/K. We also found a similar value of αK_T = 0.0033 ±0.0002 GPa/K when Holmes et al. (1989)'s Pt scale was used.

Both of the two different Pt scales yielded the very low thermal expansivity of B2 KCl. The αK_T term in this study was found to be higher than that obtained based on theoretical calculations (0.00224 GPa/K) and experiments up to 8 GPa (0.00284 GPa/K) (Walker et al. 2002; Dewaele et al. 2012) (Table 2). Note that the thermal expansivity of B2 KCl is still low compared with B2 NaCl. A DAC experiment on B2 NaCl reported a larger Grüneisen parameter γ_0 = 1.70 (Fei et al. 2007), which corresponds to αK_T = 0.0040 GPa/K. Theoretical calculations also reported small αK_T of B2 NaCl ranging from 0.00328 to 0.00468 GPa/K (Ueda et al. 2008; Ono et al. 2010). Figure 6b shows thermal pressures of B2 KCl calculated from the Mie–Grüneisen–Debye model in this study. The calculated thermal pressure is almost pressure insensitive due to the small Grüneisen parameter. This is in good agreement with Dewaele et al. (2012), in which the thermal pressure is assumed to be independent of volume.

IMPLICATIONS

In order to determine the accurate sample pressure at a high temperature in a laser-heated DAC experiment, pressure calibrants such as Pt, Au, and MgO are commonly mixed with the sample so that both materials are under the identical

252 temperature condition. However, for a study of the Earth's core materials (pure iron or its
253 alloy with light elements), this is not suitable due to the potential chemical reactions. A
254 KCl would be an alternative high-T pressure calibrant. The present study revealed that
255 KCl shows a small thermal pressure at any given pressure. For instance, the thermal
256 pressure of KCl is as small as ~10 GPa at 3000 K, then increases to ~15 GPa at 4000 K
257 regardless of the pressure, which are ~40% smaller than the case for Pt, Au, or MgO
258 (Tange et al. 2009; Yokoo et al. 2009). Such low thermal expansivity allows for
259 calculating the sample pressure on heating from the EOS of B2 KCl as a pressure
260 medium even in the case of the large temperature gradients present within KCl layers.
261 The temperature of the KCl pressure medium may be corrected downward from the
262 measured sample temperature to account for axial thermal gradients through the
263 insulating layer (Campbell et al. 2009), which will reduce the pressure uncertainty to as
264 small as a few GPa. In conclusion, the determined low thermal pressure of B2 KCl
265 validates the use of a KCl medium as a high-*T* pressure marker. This would add another
266 advantage of KCl over the other materials to the soft and chemically inert natures.

267 ## ACKNOWLEDGMENTS

268 Yoichi Nakajima is acknowledged for fruitful discussion about equation of state.
269 We also thank Haruka Ozawa for her technical assistance. Comments from an
270 anonymous reviewer were helpful to improve the manuscript. The synchrotron X-ray
271 diffraction experiments were performed at BL10XU, SPring-8 (proposal Nos.
272 2012A0087, 2012B0087 and 2013B0087). TK was supported by the European Research
273 Council (ERC) Consolidator Grant (#647723).

REFERENCES CITED

Andrault, D., Pesce, G., Bouhifd, M.A., Bolfan-Casanova, N., Hénot, J.-M., and Mezouar, M. (2014) Melting of subducted basalt at the core–mantle boundary. Science, 344, 892–895.

Anzellini, S., Dewaele, A., Mezouar, M., Loubeyre, P., and Morard, G. (2013) Melting of iron at Earth's inner core boundary based on fast X-ray diffraction. Science, 340, 464–466.

Boehler, R., Ross, M., and Boercker, D.B. (1997) Melting of LiF and NaCl to 1 Mbar: Systematics of ionic solids at extreme conditions. Physical Review Letters, *78*, 4589–4592.

Campbell, A.J. and Heinz, D.L. (1991) Compression of KCl in the B2 structure to 56 GPa. Journal of Physics and Chemistry of Solids, 52, 495–499.

Campbell, A.J., Danielson, L., Righter, K., Seagle, C.T., Wang, Y., and Prakapenka, V.B. (2009) High pressure effects on the iron–iron oxide and nickel–nickel oxide oxygen fugacity buffers. Earth and Planetary Science Letters, 286, 556–564.

Dewaele, A., Belonoshko, A.B., Garbarino, G., Occelli, F., Bouvier, P., Hanfland, M., and Mezouar, M. (2012) High-pressure-high-temperature equation of state of KCl and KBr. Physical Review B, 85, 214105.

Dorfman, S M., Prakapenka, V. B., Meng, Y., and Duffy, T.S. (2012) Intercomparison of pressure standards (Au, Pt, Mo, MgO, NaCl and Ne) to 2.5 Mbar, Journal of Geophysical Research, 117, B08210.

297 Dorogokupets, P.I., and Oganov, A.R. (2007) Ruby, metals, and MgO as alternative
298 pressure scales: A semiempirical description of shock-wave, ultrasonic, X-ray, and
299 thermochemical data at high temperatures and pressures. Physical Review B, 75,
300 024115.
301 Fei, Y., Ricolleau, A., Frank, M., Mibe, K., Shen, G., and Prakapenka, V.B. (2007)
302 Toward an internally consistent pressure scale, Proceedings of the National
303 Academy of Sciences of the United States of America, 104, 9182–9186.
304 Gray, D.E. (1963) American Institute of Physics Handbook, 2nd ed. (McGraw-Hill, New
305 York).
306 Holmes, N.C., Moriarty, J.A., Gathers, G.R., and Nellis, W.J. (1989) Equations of state of
307 platinum to 660 GPa (6.6 Mbar). Journal of Applied Physics, 66, 2962–2967.
308 Jackson, I. and Rigden, S.M. (1996) Analysis of P-V-T data: Constraints on the
309 thermoelastic properties of high-pressure minerals. Physics of the Earth and
310 Planetary Interiors, 96, 85–112.
311 Komabayashi, T., Hirose, K., Ohishi, Y. (2012) In situ X-ray diffraction measurements of
312 the fcc–hcp phase transition boundary of an Fe–Ni alloy in an internally heated
313 diamond anvil cell. Physics and Chemistry of Minerals, 39, 329–338.
314 Menéndez-Proupin, E., and Singh, A.K. (2007) *Ab initio* calculations of elastic properties
315 of compressed Pt. Physical Review B, 76, 054117.
316 Morard, G., Andrault, D., Antonangeli, D., Nakajima, Y., Auzende, A.L., Boulard, E.,
317 Cervera, S., Clark, A., Lord, O.T., Siebert, J., Svitlyk, V., Garbarino, G., and
318 Mezouar, M. (2017) Fe–FeO and Fe–Fe_3C melting relations at Earth's core–mantle
319 boundary conditions: Implications for a volatile-rich or oxygen-rich core, Earth and

Planetary Science Letters, 473, 94–103.

Ohishi, Y., Hirao, N., Sata, N., Hirose, K., and Takata, M. (2008) Highly intense monochromatic X-ray diffraction facility for high-pressure research at SPring-8. High Pressure Research, 28, 163–173.

Ono, S. (2010) The equation of state of B2-type NaCl, Jounal of Physics: Conference Series, 215, 012196.

Ono, S., Brodholt, J.P., and Price, G.D. (2011) Elastic, thermal and structural properties of platinum. Jounal of Physics and Chemistry of Solids, 72, 169–175.

Sakai, T., Ohtani, E., Hirao, N, and Ohishi, Y. (2011) Equation of state of the NaCl-B2 phase up to 304 GPa, Journal of Applied Physics, 109, 084912.

Seto, Y., Nishio-Hamane, D., Nagai, T., Sata, N. (2010) Development of a software suite on X-ray diffraction experiments. The Review of High Pressure Science and Technology, 20, 269–276.

Shim, S-H., Duffy, T.S., and Shen, G. (2000) The equation of state of $CaSiO_3$ perovskite to 108 GPa at 300 K. Physics of the Earth and Planetary Interiors, 120, 327–338.

Singh, A.K. (2009) Analysis of nonhydrostatic high-pressure diffraction data (cubic system): Assessment of various assumptions in the theory, Journal of Applied Physics, 106, 043514.

Singh, A.K., and Takemura, K. (2001) Measurement and analysis of nonhydrostatic lattice strain component in niobium to 145 GPa under various fluid pressure-transmitting media, Journal of Applied Physics, 90, 3269.

Singh, A. K., H. Liermann, Y. Akahama, S. K. Saxena, and E. Menéndez-Proupin (2008), Strength of polycrystalline coarse-grained platinum to 330 GPa and of

nanocrystalline platinum to 70 GPa from high-pressure X-ray diffraction data, Journal of Applied Physics, 103, 063524.

Sokolova, T.S., Dorogokupets, P.I., Dymshits, A.M., Danilov, B.S., and Litasov, K.D. (2016) Microsoft excel spreadsheets for calculation of *P–V–T* relations and thermodynamic properties from equations of states of MgO, diamond and nine metals as pressure markers in high-pressure and high-temperature experiments, Computers and Geosciences, 94, 162–169.

Takemura, K., and Dewaele, A. (2008) Isothermal equation of state for gold with a He-pressure medium, Physical Review B, 78, 104119.

Tange, Y., Y. Nishihara, and T. Tsuchiya (2009), Unified analyses for *P–V–T* equation of state of MgO: A solution for pressure-scale problems in high *P–T* experiments, Journal of Geophysical Research, 114, B03208.

Tateno, S., Kuwayama, Y., Hirose, K., and Ohishi, Y. (2015) The structure of Fe–Si alloy in Earth's inner core. Earth and Planetary Science Letters, 418, 11–19.

Ueda, Y., Matsui, M., Yokoyama, A., Tange, Y., and Funakoshi K. (2008) Temperature-pressure-volume equation of state of the B2 phase of sodium chloride, Journal of Applied Physics, 103, 113513.

Uts, I., Glazyrin, K., and Lee, K.K.M. (2013) Effect of laser annealing of pressure gradients in a diamond-anvil cell using common solid pressure media, Review of Scientific Instrument, 84, 103904.

Walker, D., Cranswick, L.M.D., Verma, P.K., Clark, S.M., and Buhre, S. (2002) Thermal equation of state for B1 and B2 KCl, American Mineralogist, 87, 805–812.

Yagi, T. (1978) Experimental determination of thermal expansivity of several alkali

halides. Journal of Physics and Chemistry of Solids, 39, 563–571.

Yokoo, M., Kawai, N., Nakamura, K.G., Kondo, K., Tange, Y., and Tsuchiya, T. (2009) Ultrahigh-pressure scales for gold and platinum at pressures up to 550 GPa, Physical Review B, 80, 104114.

Figure captions

FIGURE 1. Integrated XRD pattern collected (a) in situ at 1820 K and 22 GPa in run #4, where B2 KCl, Pt (pressure marker), and Ar (pressure medium) are observed. XRD patterns obtained after thermal annealing at (b) 104 GPa and (c) 229 GPa in runs #2 and #1, respectively, are also shown.

FIGURE 2. The gamma plot at selected pressures for (a) Pt and (b) B2 phase of KCl before and after thermal annealing shown in blue and red, respectively (see the text for details). The variation of lattice parameters is indicated for different (*hkl*), where a_m(*hkl*) is the measured lattice parameter calculated from individual (*hkl*), and *a* is the mean lattice parameter calculated from all reflections. The solid line is a least-squares fit to the data. According to current analysis, a_m(200) and a_m(400) for Pt and a_m(200) for B2 KCl are not used for calculating unit-cell volume.

FIGURE 3. Differential stress, *t*, and *St* value measured in (a) Pt and (b) B2 KCl, respectively, before (blue) and after (red) thermal annealing. Previous measurements of *t* values in Pt loaded in He pressure medium are also shown (gray) (Dorfman et al. 2012). Nonhydrostatic effect is clearly reduced after laser heating. The *St* values of KCl before heating at P>200 GPa are greater than |0.1| and beyond the range of the diagram.

FIGURE 4. Variation of full width at half maximum (FWHM) normalized to diffraction angle ($\Delta(2\theta)/(2\theta)$) of the most intense reflection from (111) and (110) of (a) Pt and (b) B2 KCl, respectively. Peak width before heating (blue) is reduced by laser annealing (red). Cold compression data for Pt in He medium also shown (gray) (Dorfman et al. 2012). Shadow indicates the range of FWHM of the diffraction peaks from (111) to (422) of CeO_2 standard as a reference.

FIGURE 5. (a) Volume data for B2 KCl and fit to the Vinet EoS at room temperature. Pressures are calculated from the EoS of Pt proposed by Sokolova et al. (2016). All data are collected after laser annealing. Broken line denotes previous cold compression data with He pressure medium (Dewaele et al. 2012). (b) Volume data for 300 K and high-temperature and isothermal compression curve based on the Mie–Grüneisen–Debye model.

FIGURE 6. (a) The comparison with our EoS based on various pressure scales and that obtained in Dewaele et al. (2012) calibrated by ruby pressure gauge by Dorogokupets and Oganov, 2007, which is consistent with their Pt scale. (b) Thermal pressures at different temperatures calculated from present study based on the Mie–Grüneisen–Debye model (solid line) and those from Dewaele et al. (2012) based on simple linear temperature dependence independent from volume (broken line).

TABLE 1. Unit-cell parameters of Pt and B2 KCl

					Pt			
Run	P (GPa)[a]	±	T (K)	±	a (Å)	±	V (Å^3)	±
#1	126.2	0.3	300		3.6188	0.0004	47.39	0.01
	143.7	1.3	300		3.5950	0.0017	46.46	0.07
	163.5	2.1	300		3.5704	0.0025	45.52	0.10
	189.3	1.1	300		3.5413	0.0012	44.41	0.04
	201.9	2.0	300		3.5282	0.0020	43.92	0.07
	212.2	2.2	300		3.5178	0.0022	43.53	0.08
	228.6	2.0	300		3.5021	0.0018	42.95	0.07
#2	84.8	0.3	300		3.6853	0.0006	50.05	0.02
	103.7	0.5	300		3.6528	0.0008	48.74	0.03
	119.0	0.4	300		3.6293	0.0005	47.80	0.02
#3	10.0	0.2	1640	10	3.8964	0.0003	59.16	0.01
	10.2	0.3	1780	10	3.8839	0.0005	58.59	0.02
	9.7	0.3	1480	10	3.8488	0.0004	57.01	0.02
	6.0	0.1	300		3.8097	0.0010	55.29	0.04
	14.1	0.3	2080	10	3.9040	0.0002	59.50	0.01
	9.0	0.1	300		3.9019	0.0001	59.40	0.01
	22.8	0.4	2160	30	3.8373	0.0004	56.51	0.02
	20.7	0.1	1490	10	3.8240	0.0006	55.92	0.03
	18.4	0.1	300		3.7870	0.0007	54.31	0.03
	31.6	0.5	2390	60	3.7652	0.0007	53.38	0.03
	30.1	0.1	1780	20	3.7470	0.0004	52.61	0.02
	37.0	0.2	2560	10	3.9246	0.0005	60.45	0.02
	30.6	0.3	300		3.9289	0.0003	60.65	0.01
	48.3	0.3	2390	30	3.9199	0.0005	60.23	0.02
	46.6	0.7	1790	10	3.9208	0.0005	60.27	0.02
#4	4.2	0.1	300		3.8844	0.0008	58.61	0.03
	8.7	0.9	1680	100	3.8728	0.0005	58.09	0.02
	4.7	0.0	300		3.8573	0.0005	57.39	0.02
	22.2	0.9	1820	110	3.8462	0.0003	56.90	0.01
	27.2	0.2	1890	20	3.8425	0.0012	56.73	0.05
	21.8	0.1	300		3.8028	0.0004	55.00	0.02
	31.0	0.6	1990	50	3.7950	0.0009	54.66	0.04
	25.9	0.2	300		3.9324	0.0008	60.81	0.04
	38.7	0.3	300		3.8766	0.0004	58.26	0.02

47.1	0.3	300		3.8597	0.0002	57.50	0.01
60.7	2.5	2210	210	3.8487	0.0007	57.01	0.03
58.1	1.8	1640	170	3.7660	0.0023	53.41	0.10
59.4	0.8	2300	200	3.7620	0.0013	53.24	0.05
54.7	0.2	300		3.7710	0.0019	53.63	0.08

[a]Pressure was calculated based on the equation of state proposed by Sokolova et al. (2016).

[b] t values at high temperature are calculated with elastic anisotropy factor at 300 K for refere

		B2 KCl					
t (GPa)[b]	±	a (Å)	±	V (Å^3)	±	St	±
0.92	0.32	2.8682	0.0039	23.5946	0.0957	0.0021	0.0130
0.35	0.97	2.8256	0.0014	22.5587	0.0329	0.0068	0.0029
1.82	1.49	2.7919	0.0040	21.7624	0.0946	0.0072	0.0056
0.85	1.81	2.7522	0.0027	20.8474	0.0625	0.0060	0.0021
1.40	-	2.7346	0.0009	20.4485	0.0210	-0.0114	-
0.48	1.56	2.7217	0.0004	20.1622	0.0086	0.0127	-
0.68	0.13	2.6997	0.0004	19.6761	0.0094	0.0129	-
1.00	0.26	2.9757	0.0011	26.3493	0.0297	0.0030	0.0020
0.97	0.19	2.9187	0.0005	24.8627	0.0137	0.0035	0.0010
0.81	0.43	2.8829	0.0012	23.9597	0.0300	0.0081	0.0025
0.06	0.10	3.5581	0.0008	45.0463	0.0321	0.0058	0.0026
0.14	0.11	3.4902	0.0012	42.5142	0.0428	-0.0019	0.0050
0.03	0.13	3.3543	0.0018	37.7402	0.0592	-0.0019	0.0021
0.11	0.07	3.2359	0.0016	33.8821	0.0500	-0.0018	0.0013
0.17	0.15	3.6194	0.0005	47.4154	0.0183	0.0003	0.0001
0.00	0.13	3.5984	0.0000	46.6154	0.0017	0.0011	0.0016
0.29	0.21	3.3148	0.0013	36.4220	0.0431	0.0005	0.0006
-0.11	0.08	3.2753	0.0006	35.1356	0.0183	0.0014	0.0006
0.23	0.15	3.1833	0.0018	32.2575	0.0537	-0.0021	0.0023
0.01	0.10	3.1321	0.0005	30.7265	0.0146	-0.0004	0.0011
-0.15	0.05	3.0934	0.0004	29.6002	0.0103	0.0016	0.0019
0.23	0.24	3.5717	0.0020	45.5635	0.0769	0.0004	0.0004
0.02	0.29	3.5795	0.0036	45.8620	0.1389	-0.0010	0.0028
-0.13	0.08	3.5790	0.0014	45.8456	0.0542	-0.0001	0.0007
0.17	0.41	3.5062	0.0001	43.1025	0.0035	0.0006	0.0007
0.02	0.07	3.3718	0.0004	38.3338	0.0134	0.0007	0.0009
-0.06	0.17	3.3701	0.0004	38.2765	0.0125	0.0016	0.0022
0.04	0.03	3.2952	0.0009	35.7800	0.0283	-0.0024	0.0011
-0.11	0.06	3.2905	0.0015	35.6260	0.0472	-0.0001	0.0023
-0.02	0.06	3.2497	0.0004	34.3199	0.0133	0.0024	0.0018
0.00	0.13	3.1633	0.0004	31.6537	0.0127	-0.0016	0.0016
-0.13	0.17	3.1618	0.0002	31.6079	0.0063	0.0004	0.0002
0.09	0.12	3.5952	0.0004	46.4679	0.0151	-0.0030	0.0007
0.33	0.49	3.3820	0.0013	38.6842	0.0442	-0.0004	0.0022

0.30	0.17	3.3260	0.0003	36.7925	0.0105	0.0019	0.0018
0.70	0.70	3.2870	0.0002	35.5151	0.0060	0.0024	0.0005
-0.20	0.40	3.1000	0.0008	29.7923	0.0235	0.0029	0.0014
-0.09	0.61	3.0983	0.0012	29.7421	0.0332	0.0041	0.0022
-0.27	0.13	3.0994	0.0019	29.7747	0.0539	-0.0003	0.0006

ence.

TABLE 2. Thermoelastic parameters for B2 KCl

	V_0* (Å^3)	K_0 (GPa)	±	K'_0	±	γ_0	±	q	±
This study	*Sokolova's Pt scale*								
	54.5	18.3	0.3	5.60	0.03	0.58	0.05	0.9	0.2
	54.5	18.3	0.2	5.60	0.03				
	Holmes' Pt scale								
	54.5	17.4	0.2	5.77	0.04	0.46	0.05	0.7	0.3
	54.5	17.7	0.3	5.60	0.04				
Dewaele et al. (2012)	54.5	17.2		5.89					
Walker et al. (2002)	53.53	23.7		4.4					
Campbell & Heinz (1991)	53.8	24.6		5.2					

Note : V_0 is fixed during fitting to 54.5 (Å^3) from Dewaele et al. (2012).

αK (GPa/K)	±	α (1/K)
0.0037	0.0001	
0.0033	0.0002	
0.00224		
0.00284		0.00012

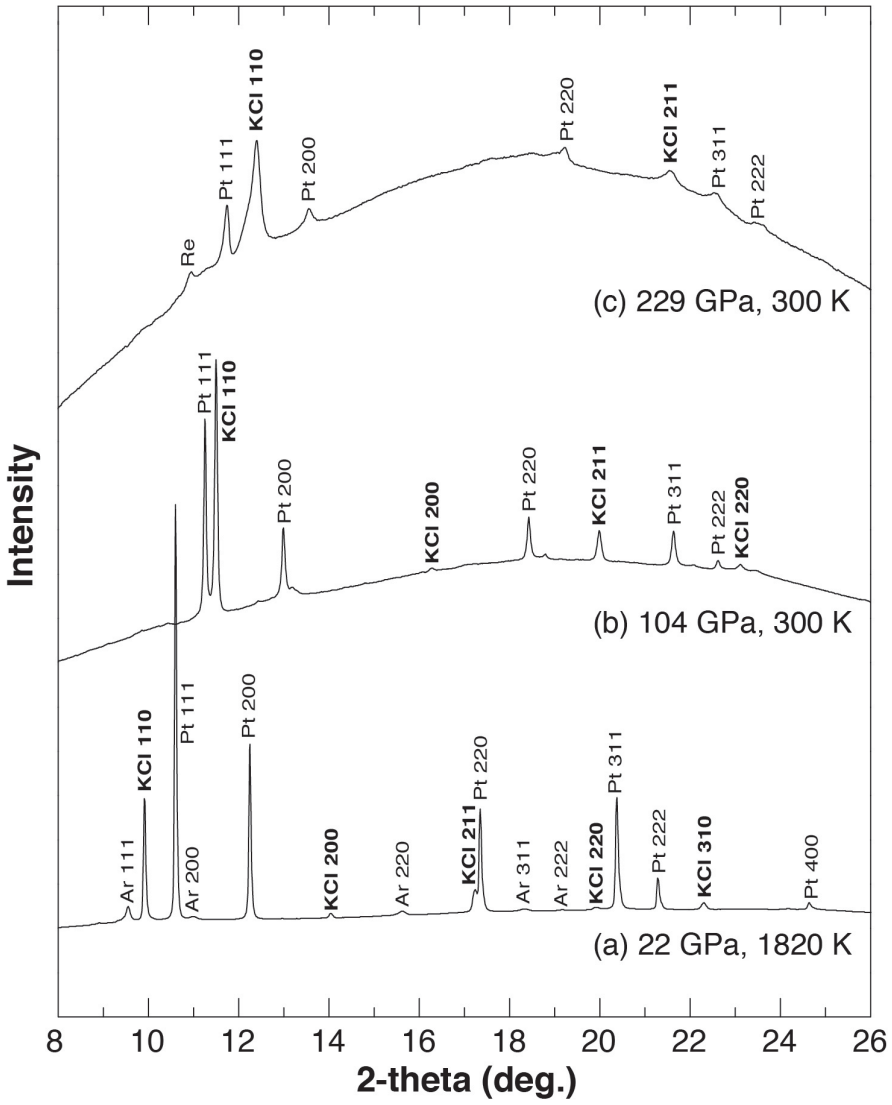
Intensity
2-theta (deg.)
8
10
12
14
16
18
20
22
24
26
(c) 229 GPa, 300 K
Re
Pt 111
KCl 110
Pt 200
Pt 220
KCl 211
Pt 311
Pt 222
(b) 104 GPa, 300 K
Pt 111
KCl 110
Pt 200
KCl 200
Pt 220
KCl 211
Pt 311
Pt 222
KCl 220
(a) 22 GPa, 1820 K
Ar 111
KCl 110
Pt 111
Ar 200
Pt 200
KCl 200
Ar 220
KCl 211
Pt 220
Ar 311
Ar 222
KCl 220
Pt 311
Pt 222
KCl 310
Pt 400

Fig. 1

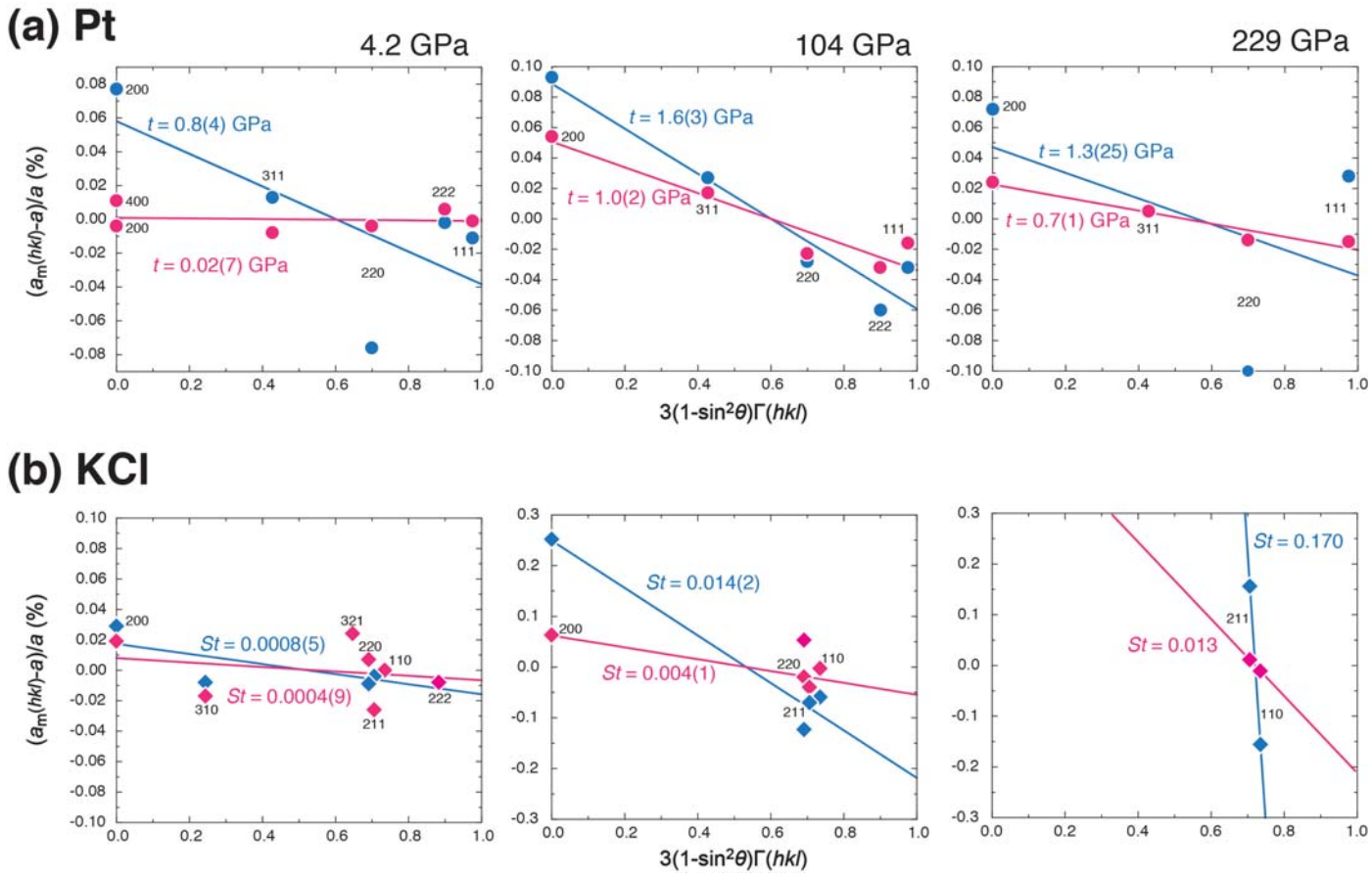
(a) Pt
4.2 GPa
104 GPa
229 GPa
t = 0.8(4) GPa
t = 0.02(7) GPa
t = 1.6(3) GPa
t = 1.0(2) GPa
t = 1.3(25) GPa
t = 0.7(1) GPa
(a_m(hkl)-a)/a (%)
3(1-sin²θ)Γ(hkl)
(b) KCl
St = 0.0008(5)
St = 0.0004(9)
St = 0.014(2)
St = 0.004(1)
St = 0.170
St = 0.013

Fig. 2

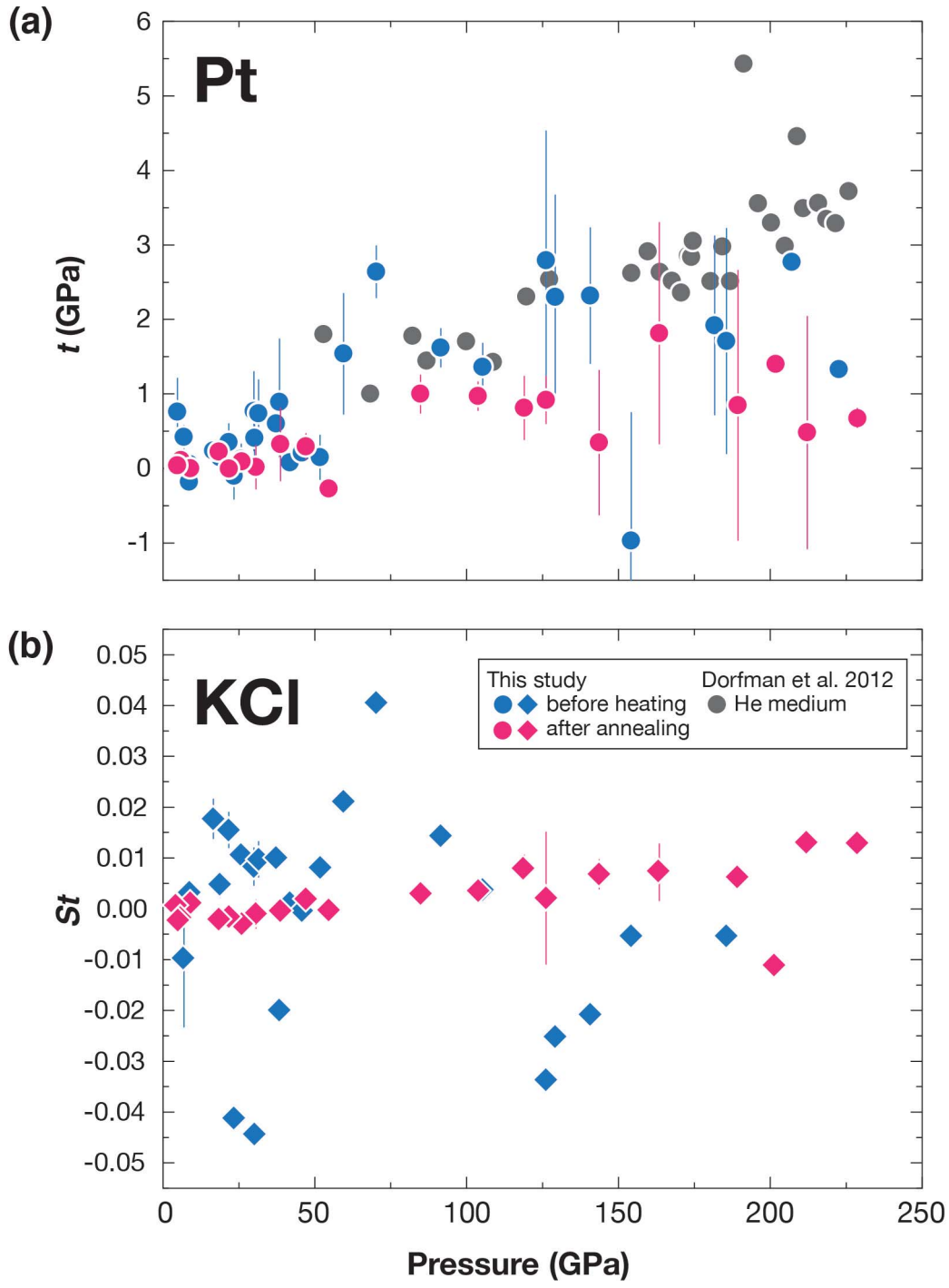
(a)
Pt
t (GPa)
6
5
4
3
2
1
0
-1
(b)
KCl
This study
before heating
after annealing
Dorfman et al. 2012
He medium
St
0.05
0.04
0.03
0.02
0.01
0.00
-0.01
-0.02
-0.03
-0.04
-0.05
0
50
100
150
200
250
Pressure (GPa)

Fig. 3

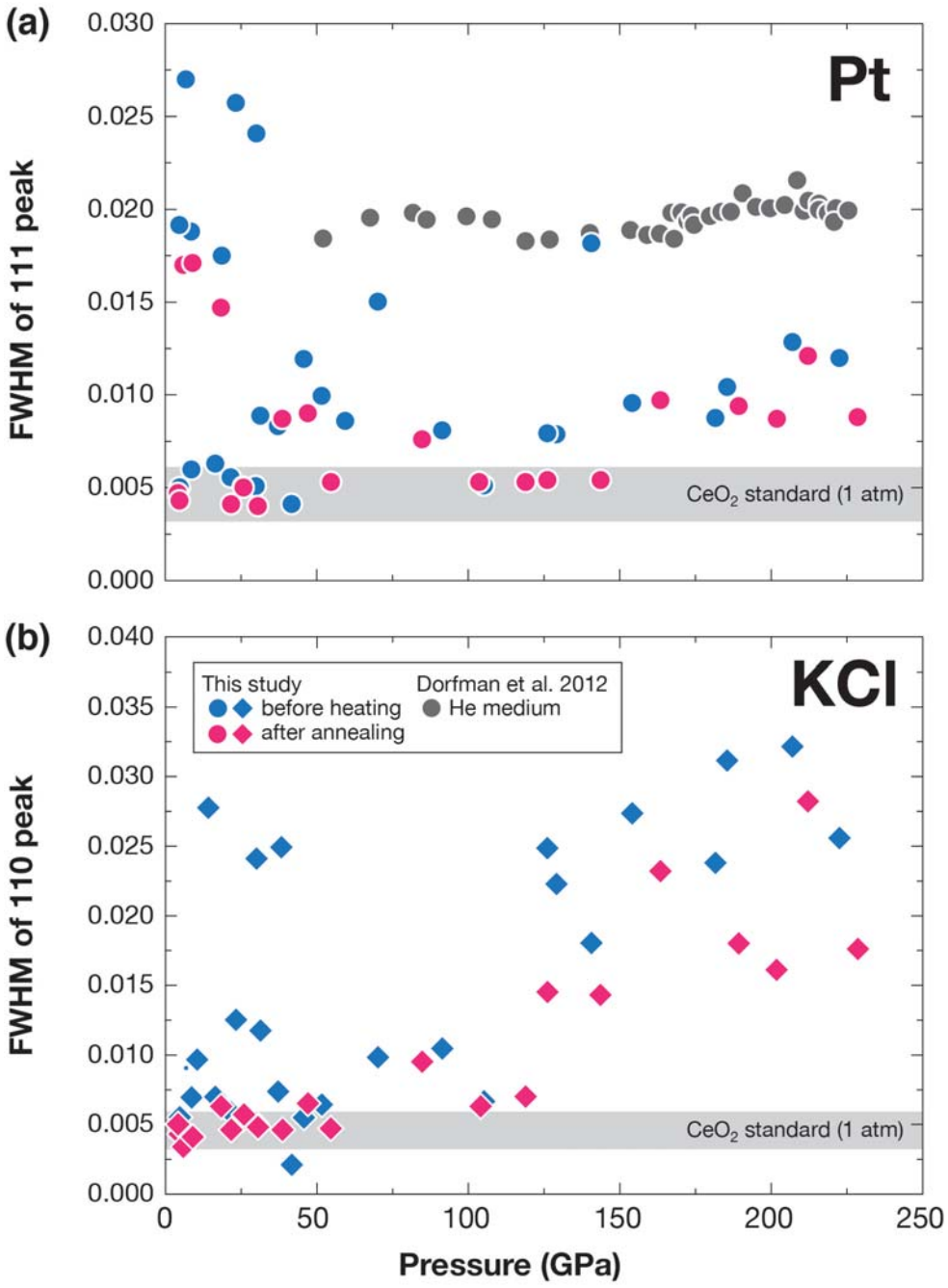
(a)
Pt
FWHM of 111 peak
0.030
0.025
0.020
0.015
0.010
0.005
0.000
CeO2 standard (1 atm)
(b)
KCl
This study
before heating
after annealing
Dorfman et al. 2012
He medium
FWHM of 110 peak
0.040
0.035
0.030
0.025
0.020
0.015
0.010
0.005
0.000
CeO2 standard (1 atm)
0
50
100
150
200
250
Pressure (GPa)

Fig. 4

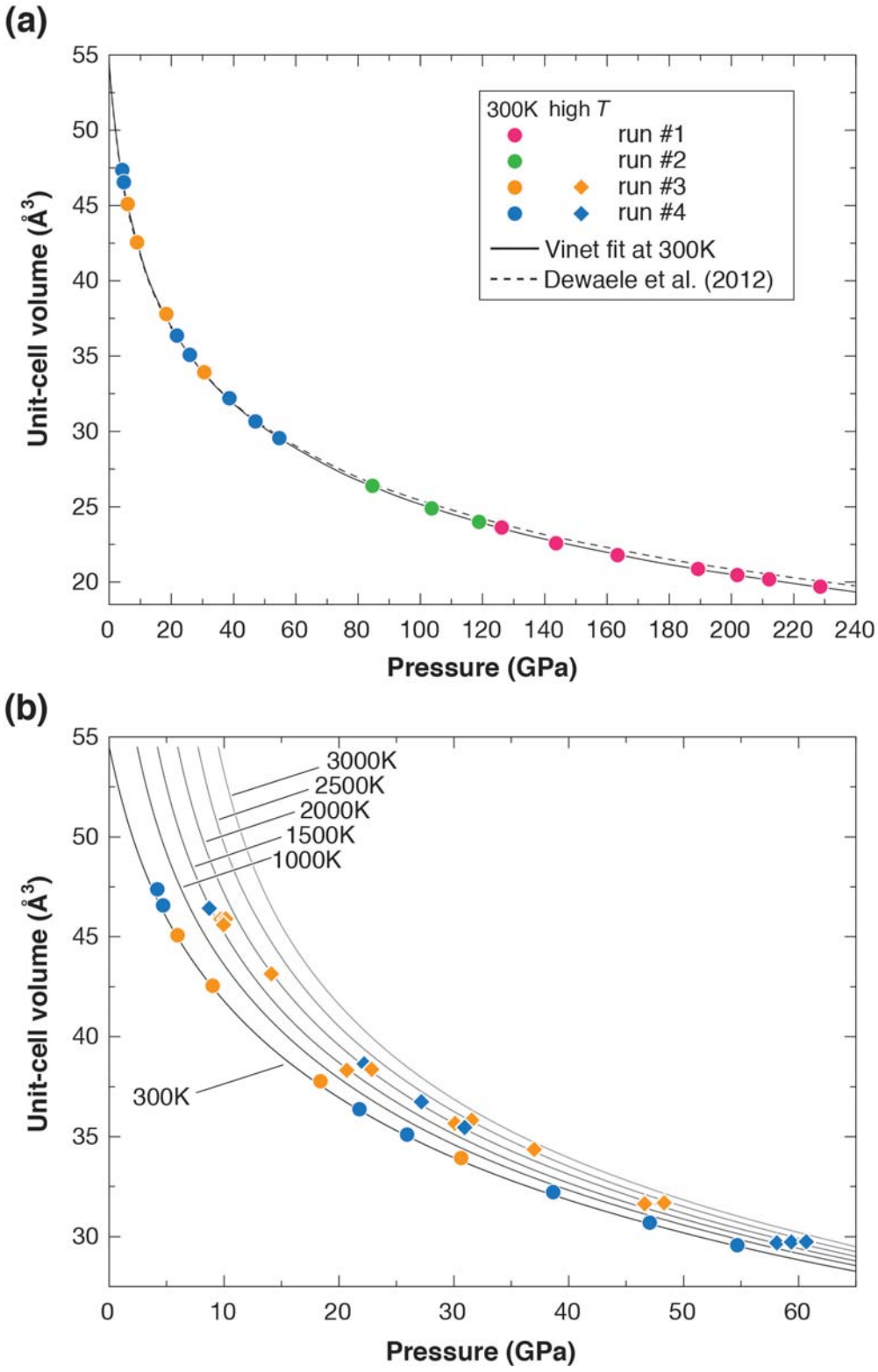
(a)
300K high T
run #1
run #2
run #3
run #4
Vinet fit at 300K
Dewaele et al. (2012)
Unit-cell volume (Å3)
Pressure (GPa)
(b)
3000K
2500K
2000K
1500K
1000K
300K
Unit-cell volume (Å3)
Pressure (GPa)

Fig. 5

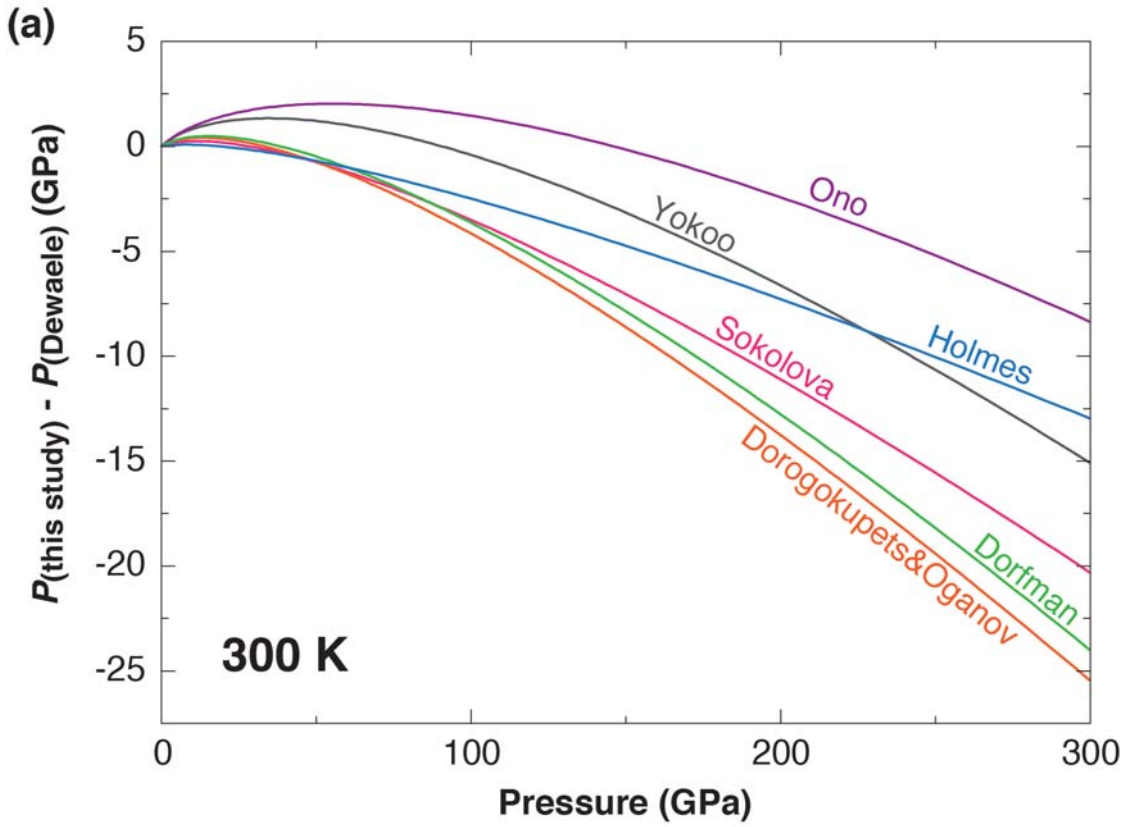
(a)
5
0
-5
-10
-15
-20
-25
P(this study) - P(Dewaele) (GPa)
Ono
Yokoo
Holmes
Sokolova
Dorogokupets&Oganov
Dorfman
300 K
0
100
200
300
Pressure (GPa)

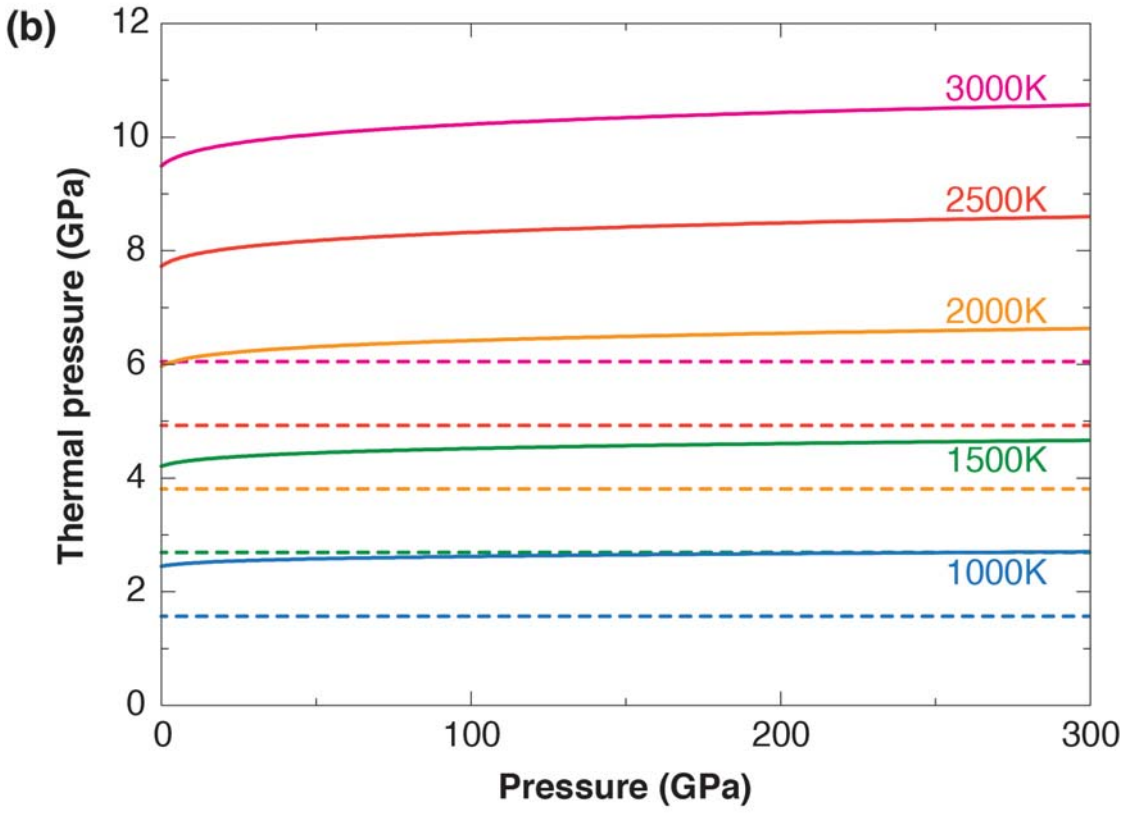
(b)
12
10
8
6
4
2
0
Thermal pressure (GPa)
3000K
2500K
2000K
1500K
1000K
0
100
200
300
Pressure (GPa)

Fig. 6